Direct flux vector control of IPM motor drives in the maximum torque per voltage speed range

Direct flux vector control of IPM motor drives in the maximum torque per voltage speed range

Invited post-ISIE10 paper

***Abstract*— The high speed operation region of Interior Permanent Magnet motor drives is investigated, with particular attention to the maximum torque per voltage operation. A technique is proposed for the control of the drive in such region, based on direct-flux field oriented vector control. The proposed control is easy to implement, does not require the accurate knowledge of the motor model and showed to be robust toward the effects of iron losses, of position estimation errors and dc-link variations. Moreover, it is suitable for operation in the inverter overmodulation range. Experimental results are provided for a 600 W IPM drive for home appliances.**

I. Introduction

Permanent magnet (PM) motors with flux weakening capability are appreciated for those applications where a constant power speed range (CPSR) is required, namely traction and spindle drives. A high CPSR can be obtained with different motor topologies, either with interior permanent magnet (IPM) or surface mounted PM (SPM) rotors associated with concentrated windings on the stator [1]. From a general point of view, independently of the magnets layout, the flux weakening capability of synchronous PM drives depends on the relationship between the motor characteristic current (1) and the drive rated current.

$$i_{ch} = \frac{\lambda_m}{L_d} \tag{1}$$

When the available current is of the same order of (1) the drive can produce a significant CPSR under the inverter voltage limit constraint, in case a proper flux-weakening control strategy is implemented. In particular, a drive with a current rating i_0 higher than the characteristic current:

$$i_0 > i_{ch} \tag{2}$$

has no theoretical upper speed limit [2] and needs a flux-weakening control strategy able to deal with the Maximum Torque per Voltage (MTPV) limit [3], that occurs over a certain speed. The value i_0 in (2) represents the maximum inverter current, that is usually the transient overload current of the motor. Those drives not fulfilling (2) have no MTPV speed range. An example of flux-weakening control trajectories is reported in Fig. 1 for an IPM motor drive, including the MTPV region. The flux-weakening control and in particular the MTPV speed range are the aim of this paper.

Throughout the last twenty-five years, most of PM synchronous motor drives have been vector current controlled in dq coordinates, synchronous to the rotor [4]. All the vector control techniques basically aimed at the Maximum Torque Per Ampere (MTPA) operation at low speed, below the voltage limit, and the maximum torque profile in flux weakening conditions at higher speeds [5]. At first, both goals have been pursued by means of current reference look-up tables [5], [6] built by manipulation of the motor magnetic model. Those strategies require an accurate motor identification and non obvious implementation [7], [8]. Moreover, parameters detuning and dc-link voltage variations cannot be handled by means of such open-loop techniques. A much simpler and effective closed-loop algorithm was then proposed for flux-weakening in [9], with a voltage control loop cascaded to the current vector control loops, but it was still not coping with the Maximum Torque Per Voltage (MTPV) speed region. To fill this gap, more complicated versions of [9] have been developed, resulting either in a mix of additional closed loops and tables [10], or in schemes of simpler implementation still heavily relying on the model [11]. All solutions appear too complicate implementation-wise for industrial applications.

Apart from being complicated in flux weakening, current vector control is very sensitive to orientation errors (e.g. encoder offset) in the MTPV region, where the controlled vector is very close to the negative d-axis, as shown in Fig. 1, and even small angle errors may lead to an undesired torque reversal. Last, when high speed core losses are significant a further complication of the model might be required [12].

On the opposite, flux vector based techniques need the estimate of the flux vector but are more suitable for flux weakening: in [13] one flux component and one current component are controlled, still in rotor coordinates, reducing the just mentioned sensitivity to orientation errors. Direct Torque Control (DTC) applied to IPM motor drives [14] directly controls the flux linkage amplitude and is very straightforward for maximum torque exploitation in flux weakening. DTC still requires model-based tables for MTPA operation at low speed

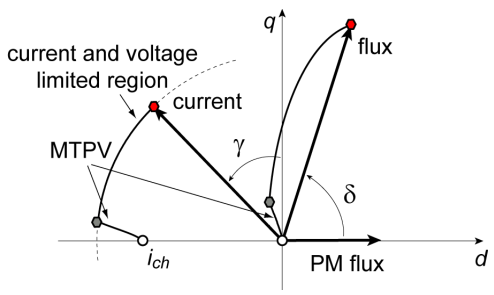

Fig. 1. Current and flux vector trajectories in flux weakening for an infinite-speed IPM motor drive.

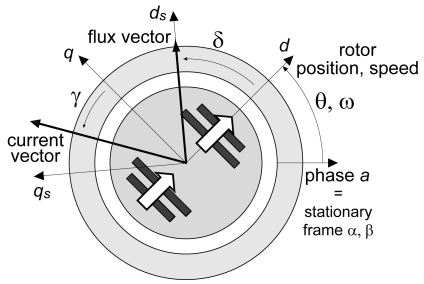

Fig. 2. Definition of the $\alpha\beta$ stator reference frame, dq rotor reference frame and d_s, q_s flux reference frame. θ is the rotor electrical position, obtained by means of an incremental encoder.

[15], as for current control, but voltage limited operation does not need any table. However, the MTPV speed range that is the aim of this paper is not addressed in DTC literature.

Direct-flux vector control (DFVC) has been proposed for IPM motor drives, aiming to combine the direct stator flux control typical of DTC and the regulation of the torque by means of one current component that is also responsible for the respect of the inverter current limit, as for current vector control [16]. DFVC is a vector control strategy implemented in the stator flux reference frame, where the two controlled components are the flux linkage amplitude and the quadrature current component. DFVC has been applied to an IPM motor drive designed for traction in [16] with limited emphasis to MTPV, showing the following advantages:

- easy control of the motor voltage in flux weakening with no need of tables of current or flux references;
- direct limitation of the maximum motor current through the control of the quadrature current reference;
- easy adaptation to a variable dc-link with no firmware modification.

In [17] the behavior of DFVC in the MTPV region has been analyzed and the closed-loop limitation of the phase angle of the flux vector to a maximum value ($\delta \leq \delta_{max}$, with δ defined in Fig. 1) has been presented as a way to control the drive in that region, with the following results:

- the MTPV speed region is well exploited with no need of knowledge of the motor model;
- the optimal δ_{max} angle is found experimentally with easy no load tests;
- iron losses are taken into account with no need of motor modeling.

In this paper, the results of [17] are reviewed and developed. In particular, a deeper insight is given to:

- the stable control in the inverter overmodulation region;
- the design of the PI regulator for controlling the maximum load angle;
- the effect of iron losses on the trajectory of the current vector.

All the considerations in the following will be referred to salient IPM motor drives, but PM motor drives with isotropic rotors can be also controlled with the proposed control technique. The results presented in the following refer to sensored control only, with the rotor position measured by means of a differential encoder.

II. Direct-flux field oriented control

The direct-flux field oriented control technique presented in [16], [17] is here briefly reviewed. The rotor and stator flux reference axes are defined in Fig. 2 where d_s, q_s are used for the stator flux oriented frame, like in stator field oriented control of IM drives.

A. Motor model in rotor coordinates dq

The model of a salient PM motor is expressed in (3-5) in the rotor reference frame.

$$\overline{v}_{dq} = R \cdot \overline{i}_{dq} + \frac{d\overline{\lambda}_{dq}}{dt} + j\omega \cdot \overline{\lambda}_{dq} \quad (3)$$

$$\overline{\lambda}_{dq} = \begin{vmatrix} L_d & 0 \\ 0 & L_q \end{vmatrix} \cdot \overline{i}_{dq} + \begin{vmatrix} \lambda_m \\ 0 \end{vmatrix} \quad (4)$$

$$T = 3/2p \cdot (\lambda_d i_q - \lambda_q i_d) \quad (5)$$

Where p is the pole-pairs, R is the stator resistance, L_d, L_q are the dq inductances, λ_m is the PM flux, T is the electromagnetic torque. Saturation and cross-saturation are not considered at the moment for keeping the equations as simple as possible, in this explanatory section. The results presented throughout the paper will refer to the experimentally identified magnetic curves of the motor under test, comprehensive of saturation and cross-saturation [18], [19]. The dq flux versus dq current components are reported in Fig. 3.

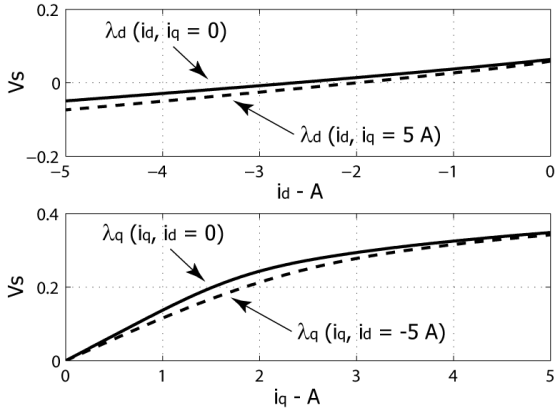

Fig. 3. dq flux components of the IPM motor under test, experimentally evaluated at a constant speed of 1500 rpm. The motor ratings are in the Appendix.

B. Motor model in flux coordinates d_s, q_s and $\lambda - i_{qs}$ torque control

In the stator flux oriented frame the motor model becomes (6-7).

$$\overline{v}_{dqs} = R \cdot \overline{i}_{dqs} + \frac{d}{dt} \begin{vmatrix} \lambda \\ 0 \end{vmatrix} + \lambda \cdot \begin{vmatrix} 0 \\ \omega + \frac{d\delta}{dt} \end{vmatrix} \quad (6)$$

$$\frac{T}{3/2 \cdot p} = \frac{1}{L_d} \cdot \left(\frac{L_d - L_q}{L_q} \lambda^2 \frac{sin2\delta}{2} + \lambda_m \lambda \cdot sin\delta \right) \quad (7)$$

Where λ is the stator flux amplitude and δ is the phase angle with respect to the d rotor axis, defined in Fig. 2. Equation (7) is formally different from the analogous one reported in [16], due to different dq axes choices here with respect to there. Both equations are correct though, coherently with the respective references. The d_s and q_s voltage equations (6) are nearly decoupled (apart from the resistive term): the flux amplitude can be regulated by means of the v_{ds} component, while the flux phase angle can be regulated by v_{qs} with very little cross interference. The electromagnetic torque depends on both state variables λ and δ and can be regulated by means of the *load angle* δ at a given flux amplitude. However, the torque versus load angle relationship is non linear and model-dependent (7). Thus, a straightforward torque control approach is suggested by the alternative expression of torque (8), that is model-independent, instead.

$$\frac{T}{3/2 \cdot p} = \lambda \cdot i_{qs} \tag{8}$$

The torque-producing current i_{qs} defined in (8) is closed-loop regulated on behalf of δ for the sake of torque control. The *Vector control* sub-block in the control scheme of Fig.6 contains two proportional-integral (PI) regulators for the closed-loop control the two selected variables: λ control is actuated by the direct voltage component v_{ds}, as said, and i_{qs} control by the quadrature voltage component v_{qs}. More details can be found in [16].

C. Maximum torque per Ampere flux reference curve

As said, the $\lambda - i_{qs}$, direct-flux vector control controls the torque by regulating the quadrature current at given flux.

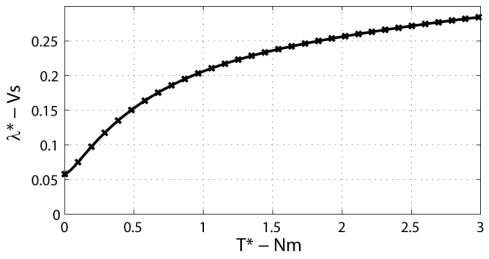

Fig. 4. Flux amplitude as a function of the torque reference for Maximum torque per Ampere operation. The curve has been obtained by manipulation of the experimental magnetic model of Fig. 3.

For a high motor efficiency at any load, it is good practice to adapt the flux amplitude setpoint to the torque setpoint, namely to reduce the flux amplitude when a low torque is requested and vice-versa. The MTPA control law maximizes the torque at given Ampere also means minimizing the copper losses, and is widely adopted in current vector controlled drives. MTPA control is implemented here by means of a look-up table that associates the correct flux amplitude to any torque request. The curve of Fig. 4 has been obtained by manipulation of the experimental magnetic curves of Fig. 3. At no load, the flux setpoint corresponds to the PM flux linkage, so that nearly no current flows into the motor phases in case zero torque is commanded. Simpler control laws, requiring less need of model manipulation than the MTPA, have been also tested in previous works [16].

D. Torque control scheme

The block scheme of the direct-flux field oriented control is reported in Fig. 6, for a speed controlled IPM motor drive. The torque setpoint determines the flux amplitude setpoint according to the MTPA look-up table, as said. The quadrature current reference i^*_{qs} is then calculated according to the torque and flux set points from (8). The flux linkage amplitude is estimated by means of the closed-loop flux observer described in the following subsection. The maximum current and maximum voltage limits are handled by two saturation blocks limiting the i_{qs} and λ references respectively, as addressed in the following.

E. Stator flux observer

The adopted reduced-order $VI\theta$ closed-loop flux observer is reported in Fig. 5 [13]. The flux estimation in stator coordinates α, β is based on the stator model (back-emf integration) at high speed and on the motor magnetic model at low speed. At steady-state, the crossover between the two models is when the motor electrical speed equals the error feedback gain: $\omega = g$ (rad/s). The magnetic model is represented in the rotor synchronous frame dq.

The simple magnetic model (4) or more accurate models as the one in Fig. 3, including saturation and cross-saturation, can be implemented, according to how accurately has the motor been identified.

With a simplified motor model as the one in (4) the control performance can deteriorate at low speed. However, even with a poor model, the phase current limit is still respected and the worst possible side effect might be a difference between the controlled torque and the torque set point. For instance: if the flux amplitude is overestimated due to an imprecise magnetic model, the actual flux will be lower than expected, and so will be the actual torque, lower then its setpoint. In case the flux phase angle is mis-estimated, the d_s, q_s reference frame is misaligned and the controlled i_{qs} is not in quadrature with the actual motor flux. Also in this case the torque will be different from the setpoint. Above the crossover frequency ($\omega > g$), the flux observer and thus the control are insensitive to the motor model (apart from the stator resistance) and include the effect of core losses with no model complication.

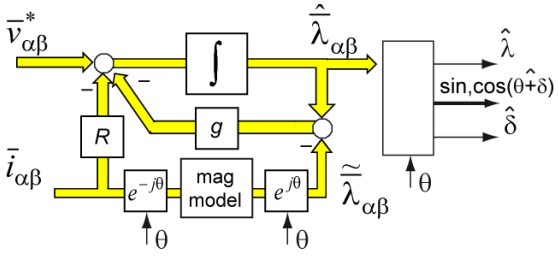

Fig. 5. Adopted flux observer.

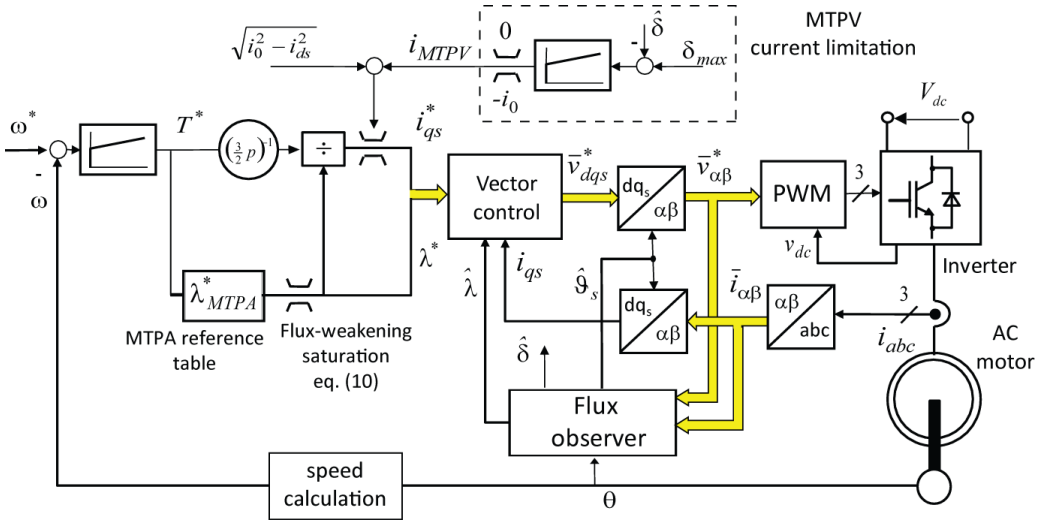

Fig. 6. Direct-flux field oriented control scheme, with the proposed MTPV limitation of the i_{qs} current put in evidence.

F. Current and voltage limitation

The motor phase current is kept under the rated value i_0 by limiting the q_s current reference according to (9).

$$i_{qs}^* \leq \sqrt{i_0^2 - i_{ds}^2} \tag{9}$$

The voltage limit is respected by reducing the reference flux linkage according to the simplified flux-weakening law (10).

$$\lambda^* \leq \frac{V_{max} - R \cdot i_{qs} \cdot sign(\omega)}{|\omega|} \tag{10}$$

where V_{max} can be updated in real time according to the measured dc-link voltage in case it is variable. $sign(\omega)$ accounts for the resistive drop reversal in braking operation with respect to motoring [20], [21].

G. Limits of operation the $\lambda - i_{qs}$ control

The torque versus δ relationship (7) is monotonic in a limited interval around $\delta = 0$: either for positive or negative values of δ (read torque) there is a maximum absolute value of the load angle δ_{max} where the torque at given flux amplitude is maximum. Over δ_{max} the torque tends to drop. This is the well known *pull-out torque* or Maximum Torque per Voltage (MTPV) condition [16]. If the load angle trespass the limit an eventual torque request tends to further increase the angle itself through the i_{qs} PI regulator: more and more v_{qs} is accumulated in case the i_{qs} error is not zero, and v_{qs} means δ derivative, according to (6). Out of the $\pm\delta_{max}$ boundary the $\lambda - i_{qs}$ control becomes unstable. Therefore, the limitation of $|\delta|$ is needed for a stable torque control, and the proper limit δ_{max} must be selected for exploiting the MTPV region at its best [17], as will be seen in section III.

III. Motor drive under test and MTPV control

The IPM motor under test, whose ratings are reported in the Appendix, has been identified according to the procedure described in [19]: the dq flux model, complete of cross saturation, has been experimentally evaluated at steady-state in the range $i_d = -5 \div 0A, i_q = 0 \div 5A$ as reported in Fig. 3.

The control trajectories of Fig. 7 have been calculated by manipulation of the experimental magnetic model in the dq current and flux planes respectively. The MTPA, $|\bar{i}| = i_0$ and MTPV curves are represented in the two planes and the characteristic current i_{ch} results to be nearly 2 A. In the dq flux plane the MTPV trajectory is well approximated by a line with constant δ angle that is $\delta_{max} = 126°$.

The expected power profile with 280 V dc-link and 5 A (pk) phase current has also been calculated according to the experimental mode and reported in Fig. 8. The MTPV speed range is above the point called B in the figure, that is from 6500 rpm on. Being the motor identification run at constant low speed (1500 rpm) the effects of iron losses are not considered in the model-based control trajectories of Fig. 7 and neither in the forecast power curve, as will be shown by experiments.

A. MTPV and maximum load angle

The derivative of the torque expression (7) with respect to δ is:

$$\frac{dT}{d\delta} = \frac{3}{2} \cdot p \cdot \left(\frac{\lambda_m}{L_d} \cdot \lambda \cdot cos\delta - \frac{L_q - L_d}{L_d L_q} \cdot \lambda^2 \cdot cos2\delta \right) \tag{11}$$

By imposing (11) to zero, the maximum torque per flux amplitude condition is found, that defines the MTPV load angle δ_{max}.

$$\lambda_m \cdot cos\delta_{max} = \frac{L_q - L_d}{L_q} \cdot \lambda \cdot cos2\delta_{max} \tag{12}$$

The solution of the implicit equation (12) depends on the motor parameters, namely the relationship between the motor saliency, represented by the $(L_q - L_d)$ term and the PM flux. For instance, a non salient motor would have $\delta_{max} = 90°$, while a salient PM motor has in general $90° < \delta_{max} <$

135°, being 135° the case of a synchronous reluctance motor. Magnetic saturation is not included in (4) and (12) but still a good analytical estimation of δ_{max} is possible, based on the simplified magnetic model: the L_d and L_q values must be identified with the current vector close by the negative d axis, with an amplitude greater than the motor characteristic current (1), or short-circuit current, as it is in the MTPV operating region.

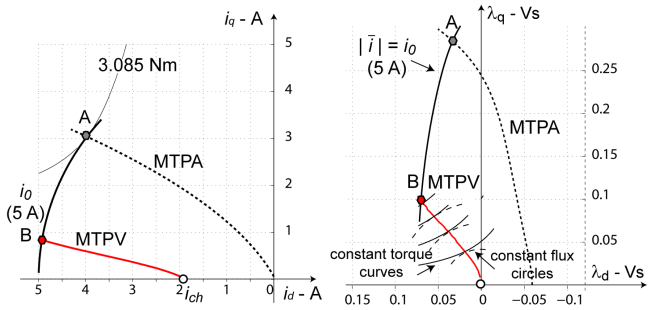

(a) current plane (b) flux plane

Fig. 7. Control trajectories in the dq current and flux planes for the drive under test, according to the steady-state identification of the IPM motor.

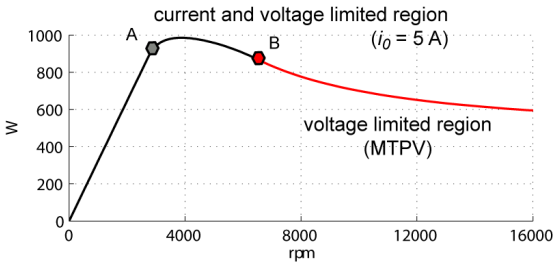

Fig. 8. Maximum power profile of the IPM motor drive under test, according to the steady-state identification of the IPM motor, with 5 A (pk) and 160 V (phase pk).

B. δ_{max} limitation strategy

The *MTPV current limitation* block, enclosed in a dashed box in Fig. 6 consists of a proportional-integral (PI) regulator that temporarily kills the q_s current in case the observed flux phase angle exceeds the set point δ_{max}. The i_{qs} saturation level (9) is corrected by means of the negative component i_{MTPV}, until the condition $\hat{\delta} = \delta_{max}$ is fulfilled. The upper limit of the PI regulator output is set to zero, that means that when $\hat{\delta} < \delta_{max}$ the MTPV block is off. In other words, the $\lambda - i_{qs}$ control switches to a $\lambda - \delta$ control, with a fixed set point of δ, in the MTPV region.

It has been reminded that without the i_{MTPV} current limitation, the $\lambda - i_{qs}$ control would be unstable in the MTPV region [16], [17]. The additional, PI-based i_{MTPV} term makes the control stable independently of the choice of δ_{max}, as demonstrated by experiments in section IV.

C. Tuning of the δ_{max} limitation regulator

The tuning of the PI regulator parameters and the bandwidth of the maximum δ limitation can be evaluated according to the simplified block scheme of Fig. 9. The inverter and flux observer dynamics have been assumed ideal. The closed loop bandwidth of the δ limitation is:

$$\omega_{bw,\delta} = \frac{k_{p,\delta} \cdot k_{p,iqs}}{\lambda} \tag{13}$$

Where $k_{p,\delta}$ and $k_{p,iqs}$ are the gains of the proportional part of the δ and i_{qs} regulators respectively. The bandwidth is variable with the flux amplitude at denominator and must be set according to its minimum value that corresponds to the maximum speed condition. As shown in the following, the PI-based δ_{max} control overcomes the instability problems of λ - i_{qs} control with any δ_{max} set-point, properly or improperly selected.

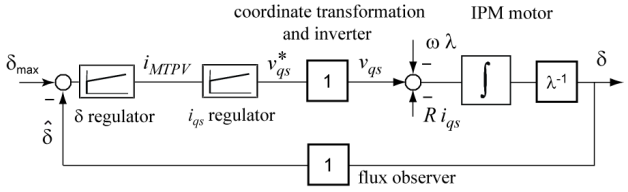

Fig. 9. Simplified block scheme representing the dynamics of the maximum δ angle regulation.

Another key condition to be respected in the design of the PI regulator is that the output span of i_{MTPV} must be as large as possible in order to keep δ_{max} control in all situations, including transients, thus the lower limit of i_{MTPV} has been set to the full current amplitude $-i_0$.

IV. Experimental Results

The IPM motor drive (specified in the Appendix) has been tested at no load in the range from zero the 16000 rpm, in motoring and braking. The flux weakening limitation (10) is set according to the real-time measure of the dc-link voltage. The overmodulation region of the inverter can be exploited or not via the V_{max} setting in (10), as shown in the following.

A. Step response from zero to 16000 rpm

The speed step response from zero to 16000 rpm at no load is reported in Fig. 10. The controlled variables $\hat{\lambda}, i_{qs}$ are reported, together with their respective reference values. The MTPV current-weakening component i_{MTPV} is reported in the i_{qs} plot, showing to be triggered from 5000 rpm on. The load angle limit is set to $\delta_{max} = 126°$. The steady-state voltage saturation actuated by the flux-weakening block is set to $V_{max} = 0.655 \cdot V_{dc}$, being V_{dc} the measured dc-link voltage, that is 14% over the theoretical limit of the inverter linear behavior ($0.577 \cdot V_{dc}$). Such $0.655 \cdot V_{dc}$ factor has been chosen as a compromise value between the above said linear limit (0.577) and the six-step operation, that would give a fundamental output voltage of $4/\pi \cdot V_{dc}/\sqrt{3} = 0.735 \cdot V_{dc}$, neglecting the inverter voltage drops. The choice of a lower

value (0.655 instead of 0.735) is made for taking into account the inverter drops and still have a voltage margin for transient regulation.

Fig. 11 shows that the voltage vector amplitude is saturated by the inverter phase voltage limitation as the vector travels along an hexagonal trajectory. The noise on the i_{qs} trace is a consequence of overmodulation, that distorts the linked flux amplitude and makes the torque control more nervous. However, no audible noise has been reported during the tests due to this reason. Moreover, due to the passive rectified, single-phase input supply, the dc-link shows a 100 Hz voltage ripple during the drive acceleration (Fig. 11). The saturated voltage hexagon varies according to, as underlined by bold red arrows in both subplots of the figure. The voltage vector trajectory in Fig. 11 and in the following have been reconstructed from the V_{dc} measure and the phase duty-cycles.

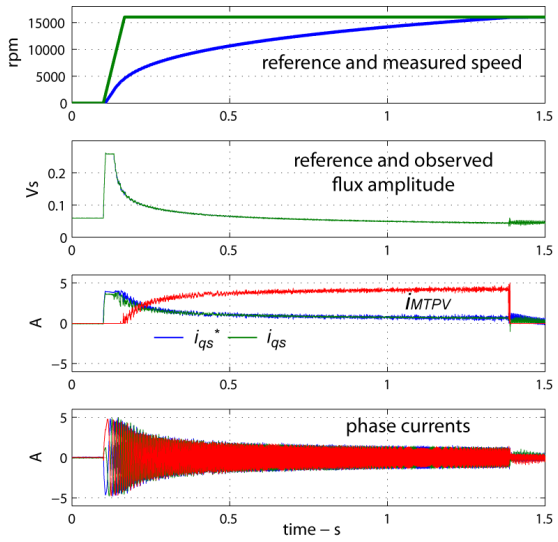

Fig. 10. Speed step response, λ and i_{qs} control trajectories, and motor phase currents. $\delta_{max} = 126°$. The current weakening component i_{MTPV} is reported in the i_{qs} subplot.

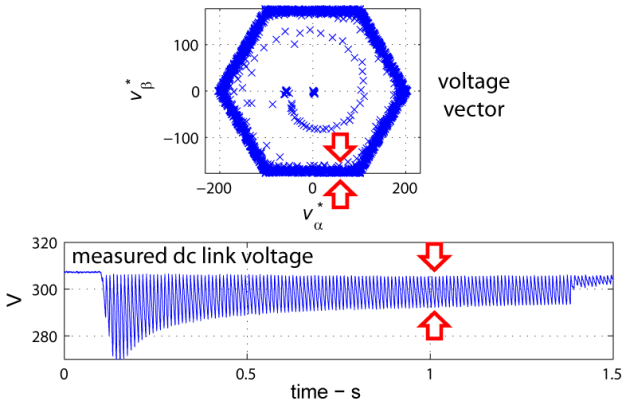

Fig. 11. Reference voltage vector and measured dc-link voltage during the step transient of Fig. 10.

B. Inverter overmodulation

As said, the exploitation of the overmodulation range is very straightforward and model-independent, and does not compromise the control stability. In Fig. 12 a detail between 0.11 s and 0.2 s of the speed step response of Figs. 10-11 is referred to as *test 1* for comparison with the response obtained with V_{max} reduced by 20% (*test 2*). The reference voltage amplitude of *test 2* is lower and its trajectory is nearly circular. The flux-weakening of *test 2* triggers at a lower speed, therefore the speed transient is slightly delayed from 3000 rpm on. The comparative test confirms that the overmodulation range is effectively giving a bit more of voltage amplitude in *test 1* and that the flux weakening control law can be adapted very easily to the requirements of the different possible applications.

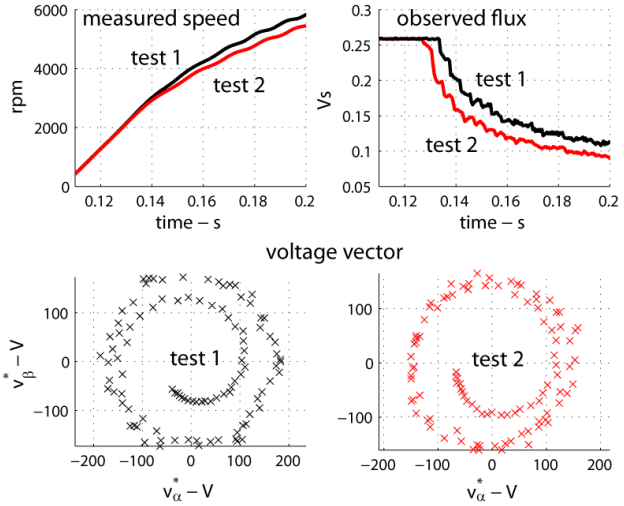

Fig. 12. Exploitation of the inverter overmodulation range: test 1 is the one reported in Figs. 10-Fig. 11, with $V_{max} = 0.655 \cdot V_{dc}$. Test 2 is with $V_{max} = 0.55 \cdot V_{dc}$.

C. Selection of the correct δ_{max}

The optimal δ_{max} value can be either evaluated analytically (12) or, in case the model is not known accurately, on the field. At this purpose, a series of tests has been performed with different δ_{max} tentative values, with the aim of obtaining the fastest possible speed step acceleration from zero to 16000 rpm: the fastest speed response corresponds to the optimal δ_{max}.

As a general procedure, the first tentative value of δ_{max} could be evaluated through (12) and the available L_d and L_q values. Otherwise, with no idea of the machine saliency, a good starting value can be either $\delta_{max} = 90°$ (PM, non salient machine) and then increase the angle or $\delta_{max} = 135°$ (synchronous reluctance machine, no PM flux) and then decrease the angle. If the first value is in between, it is necessary to test both directions (increasing and decreasing) to find out where to move to reach the fastest speed response.

The speed step response of the drive at no load is reported in Fig. 13 for five different δ_{max} values: 110°, 126°, 140°, 150° and 160°. As expected, $\delta_{max} = 110°$ is far from the

MTPV and produces a reduced torque at high speed and then the slowest speed transient overall. In fact it is $\delta_{max} = 126°$ that best approximates the MTPV curve of Fig. 7b, by the experimental model. Further details are in [17]. Still, the best speed dynamics is not obtained with $\delta_{max} = 126°$ but instead with 140°, that is over the MTPV theoretical angle. Higher values (150° and 160°) give a speed response that is very close to the optimal one. The transient trajectories of the observed flux phase angle are reported for $\delta_{max} = 126°$ and $\delta_{max} = 140°$ the two cases in Figs. 14, 15, respectively, and compared with the experimental model curves of Fig. 7.

Looking at the flux vector plots (Fig. 14b and Fig. 15b) in both cases the distortion of the flux trajectory is due to the inverter overmodulation and the variable dc-link voltage already reported. Despite such effects, the $\delta = \delta_{max}$ operation is very smooth and regular. The δ_{max} control has shown to be stable for any $\delta_{max} < 180°$. Higher values up to $\delta_{max} = 170°$ have been successfully tested giving no problem in terms of stability.

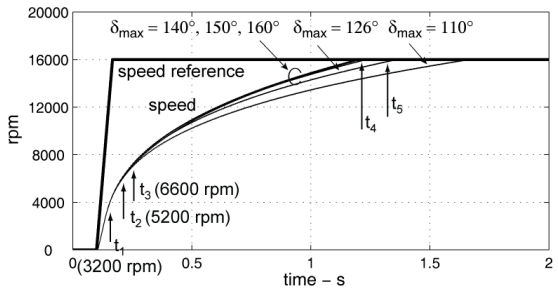

(a) speed transient

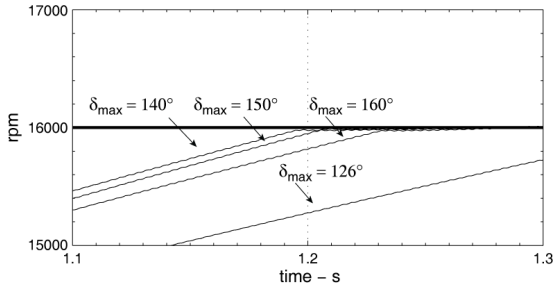

(b) detail of the speed transient

Fig. 13. Speed step response. Different δ_{max} values are evaluated in the range 100° to 160°, for selecting the one that leads to the maximum acceleration. The $t_1, ..t_5$ labels of sub-figure (a) are recalled in Figs. 14-15. Sub-figure (b) is the zoom between 1.1 s and 1.3 s, for clarity.

D. Core losses

The presence of significant iron losses is pointed out by the no load current at 16000 rpm that is around 0.5 A both in Fig. 14a (circle labelled $t > t_5$) and Fig. 15a (circle labelled $t > t_4$). This additional current component modifies the expression of torque with respect to (8) and then the current control trajectories at high speed. Iron losses can be modeled by means of a shunt current component that is part of the motor stator current but does not contribute to torque and it is impossible to be controlled directly. With current vector control, the control

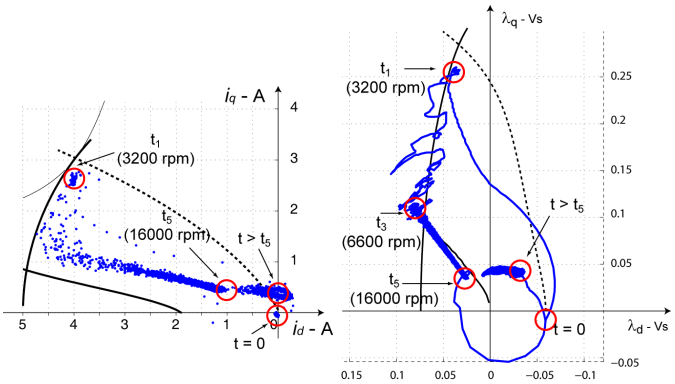

(a) current plane (b) flux plane

Fig. 14. $\delta_{max} = 126°$: trajectory of the observed flux in the dq rotor frame during the speed step transient of Fig. 13. The circles t_1, t_3 and t_5 make reference to Fig. 13.

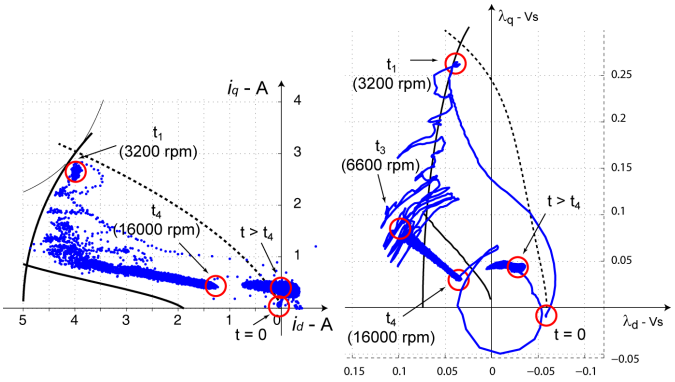

(a) current plane (b) flux plane

Fig. 15. $\delta_{max} = 140°$: trajectory of the observed flux in the dq rotor frame during the speed step transient of Fig. 13. The circles t_1, t_3 and t_5 make reference to Fig. 13.

reference trajectories should be modified according to a more complicate motor modeling, based on lumped shunt resistors in both d and q rotor directions [12]. In both Figs. 14a-15a the current trajectories are far from the steady-state, low speed evaluated MTPV line. With $\delta_{max} = 140°$ the current vector trajectory is much closer to the MTPV than in the other case. This is partially due to the massive impact of the iron loss current. Another reason contributing to the displacement of the control trajectory is the 100 μs sampling time delay, that is not negligible with respect to the electrical period at 16000 rpm.

E. Speed reversal

A speed reversal test is reported in Fig. 16. As expected, the deceleration phase is faster than the acceleration due to the combined effect of losses and of a higher dc-link: losses tend to brake both in acceleration and deceleration and the dc-link voltage is clamped to 330 V by a braking resistor with the drive regenerating. The higher available dc voltage result in a higher flux setting in flux weakening and then in a higher braking torque.

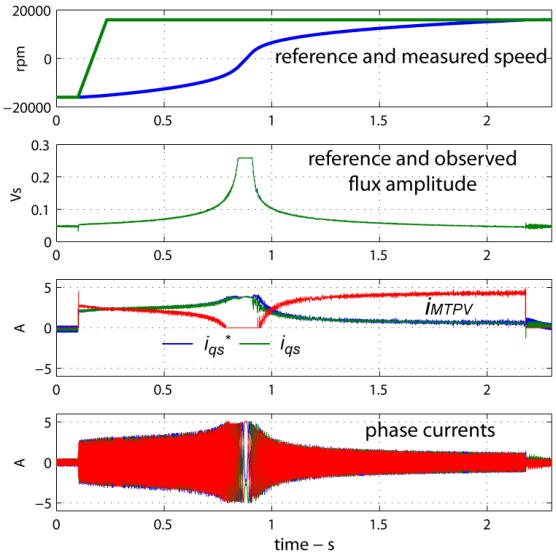

Fig. 16. Speed reversal step response, λ and i_{qs} control trajectories, and motor phase currents. $\delta_{max} = 126°$. The current weakening component i_{MTPV} is reported in the i_{qs} subplot.

V. Conclusion

The paper presents a solution for the control of IPM motor drives in the MTPV region, based on direct flux field oriented vector control. The observed phase angle of the stator flux is limited within a maximum value δ_{max} by means of a PI controller. The tuning of the additional PI controller has been addressed. The proper δ_{max} value can be found analytically or by trial and error if the motor model is not known accurately. The control is stable also in overmodulation and it is capable to follow dc-link variations even in presence of fast transients such as the 100 Hz ripple due to a single-phase AC source with passive rectifier stage.

Appendix: IPM drive ratings

The motor under test is rated: 600 W, 160 V (phase, pk), 5 A (pk), 2 pole-pairs, 16000 rpm max. $R = 8\ \Omega$, $L_d = 25$ mH, $L_q = 130$ mH (unsat), 100 mH (sat, rated current). The inverter rating is: $220V$, $50Hz$ single-phase input, passive rectifier with braking resistance. IGBT SOA: $600V$, $10A$. Dead-time setting is $1\mu s$. The switching frequency is $10kHz$.

References

[1] A. EL-Refaie and T. Jahns, "Comparison of synchronous pm machine types for wide constant-power speed operation: converter performance," *Electric Power Applications, IET*, vol. 1, no. 2, pp. 217–222, March 2007.

[2] W. Soong and T. Miller, "Field-weakening performance of brushless synchronous ac motor drives," *Electric Power Applications, IEE Proceedings -*, vol. 141, no. 6, pp. 331–340, Nov 1994.

[3] S. Morimoto, "Ipm vector control and flux weakening," in *TUTORIAL COURSE NOTES - Design, Analysis, and Control of Interior PM Synchronous Machines - IEEE Industry Applications Society Annual Meeting*, 2004.

[4] T. M. Jahns, G. B. Kliman, and T. W. Neumann, "Interior permanent-magnet synchronous motors for adjustable-speed drives," *Industry Applications, IEEE Transactions on*, vol. IA-22, no. 4, pp. 738 –747, july 1986.

[5] T. M. Jahns, "Flux-weakening regime operation of an interior permanent-magnet synchronous motor drive," *Industry Applications, IEEE Transactions on*, vol. IA-23, no. 4, pp. 681 –689, july 1987.

[6] S.Morimoto, Y.Takeda, T.Hirasa, and K.Taniguchi, "Expansion of operating limits for permanent magnet motor by current vector control considering inverter capacity," *IEEE Transactions on Industry Applications*, vol. 26, no. 5, pp. 678–690, 1990.

[7] C. Jo, J.-Y. Seol, and I.-J. Ha, "Flux-weakening control of ipm motors with significant effect of magnetic saturation and stator resistance," *Industrial Electronics, IEEE Transactions on*, vol. 55, no. 3, pp. 1330 –1340, March 2008.

[8] B. Cheng and T. Tesch, "Torque feedforward control technique for permanent-magnet synchronous motors," *Industrial Electronics, IEEE Transactions on*, vol. 57, no. 3, pp. 969 –974, March 2010.

[9] J.Kim and S.Sul, "Speed control of interior permanent magnet synchronous motor drive for the flux weakening operation," *IEEE Transactions on Industry Applications*, vol. 33, no. 1, pp. 43–48, 1997.

[10] B.-H. Bae, N. Patel, S. Schulz, and S.-K. Sul, "New field weakening technique for high saliency interior permanent magnet motor," in *Industry Applications Conference, 2003. 38th IAS Annual Meeting. Conference Record of the*, vol. 2, Oct. 2003, pp. 898–905 vol.2.

[11] Y.-D. Yoon, W.-J. Lee, and S.-K. Sul, "New flux weakening control for high saliency interior permanent magnet synchronous machine without any tables," in *Power Electronics and Applications, 2007 European Conference on*, sept. 2007, pp. 1 –7.

[12] L. Xu, X. Xu, T. Lipo, and D. Novotny, "Vector control of a synchronous reluctance motor including saturation and iron loss," *Industry Applications, IEEE Transactions on*, vol. 27, no. 5, pp. 977–985, Sep/Oct 1991.

[13] A. Vagati, M. Pastorelli, and G. Franceschini, "High-performance control of synchronous reluctance motors," *Industry Applications, IEEE Transactions on*, vol. 33, no. 4, pp. 983–991, Jul/Aug 1997.

[14] M. Rahman, L. Zhong, and K. W. Lim, "A direct torque-controlled interior permanent magnet synchronous motor drive incorporating field weakening," *Industry Applications, IEEE Transactions on*, vol. 34, no. 6, pp. 1246 –1253, nov/dec 1998.

[15] L. Tang, L. Zhong, M. Rahman, and Y. Hu, "A novel direct torque controlled interior permanent magnet synchronous machine drive with low ripple in flux and torque and fixed switching frequency," *Power Electronics, IEEE Transactions on*, vol. 19, no. 2, pp. 346 – 354, march 2004.

[16] G. Pellegrino, E. Armando, and P. Guglielmi, "Direct flux field-oriented control of ipm drives with variable dc link in the field-weakening region," *Industry Applications, IEEE Transactions on*, vol. 45, no. 5, pp. 1619–1627, Sept.-Oct. 2009.

[17] ——, "Direct-flux field-oriented control of ipm motor drives with robust exploitation of the maximum torque per voltage speed range," in *Industrial Electronics (ISIE), 2010 IEEE International Symposium on*, July 2010, pp. 1271 –1277.

[18] N.Bianchi and S.Bolognani, "Magnetic models of saturated interior permanent magnet motors based on finite element analysis," in *Proc. of IEEE Industry Applications Society Annual Meeting*, vol. 1, 1998, pp. 27 – 34.

[19] A.Vagati, M.Pastorelli, F.Scapino, and G.Franceschini, "Impact of cross saturation in synchronous reluctance motors of the transverse-laminated type," *IEEE Transactions on Industry Applications*, vol. 36, no. 4, pp. 1039 – 1046, 2000.

[20] S.-M. Sue and C.-T. Pan, "Voltage-constraint-tracking-based field-weakening control of ipm synchronous motor drives," *Industrial Electronics, IEEE Transactions on*, vol. 55, no. 1, pp. 340 –347, jan. 2008.

[21] M. Tursini, E. Chiricozzi, and R. Petrella, "Feedforward flux-weakening control of surface-mounted permanent-magnet synchronous motors accounting for resistive voltage drop," *Industrial Electronics, IEEE Transactions on*, vol. 57, no. 1, pp. 440 –448, jan. 2010.

[22] Y.-S. Kim and S.-K. Sul, "Torque control strategy of an ipmsm considering the flux variation of the permanent magnet," in *Industry Applications Conference, 2007. 42nd IAS Annual Meeting. Conference Record of the 2007 IEEE*, Sept. 2007, pp. 1301 –1307.

[23] G. Rang, J. Lim, K. Nam, H.-B. Ihm, and H.-G. Kim, "A mtpa control scheme for an ipm synchronous motor considering magnet flux variation caused by temperature," in *Applied Power Electronics Conference and Exposition, 2004. APEC '04. Nineteenth Annual IEEE*, vol. 3, 2004, pp. 1617–1621 Vol.3.